Journal of Materials Science: Materials in Electronics (2018) 29:7233–7238
https://doi.org/10.1007/s10854-018-8712-1

Effects of Al substitution on the properties of NiZnCo ferrite nanopowders

Le-Zhong Li[1] · Xiao-Xi Zhong[1] · Rui Wang[1] · Xiao-Qiang Tu[1] · Lei He[1]

Received: 26 September 2017 / Accepted: 31 January 2018 / Published online: 2 February 2018
© Springer Science+Business Media, LLC, part of Springer Nature 2018

Abstract
Al-substituted NiZnCo ferrite nanopowders, $Ni_{0.4}Zn_{0.5}Co_{0.1}Al_xFe_{2-x}O_4$ ($0 \le x \le 0.20$), were synthesized by sol–gel auto-combustion method. The influence of Al-substituted NiZnCo ferrite nanopowders on the structural and electromagnetic properties have been studied. The results of TG–DTA show that the precursor decomposition and ferrite formation occurs around 220 °C. The XRD data shows that the lattice constant, nanopowder size and X-ray theoretical density decrease with Al concentration increasing. *M*s increases with Al concentration increasing when $x \le 0.10$, and then decreases when $x > 0.10$. At the same time, *H*c decreases with Al concentration increasing when $x \le 0.10$, and then increases when $x > 0.10$. The Néel temperature decreases with Al substitution increasing. The temperature dependence of dc resistivity of the ferrite nanopowders shows the metal–semiconductor transition behavior. And the influence of Al substitution on the temperature dependence of dc resistivity is investigated.

1 Introduction

The distinct properties of ferrite nanopowders have caused more interest in the science community because high surface to volume ratio resulting in novel phenomena's of nanomagnetism such as superparamagnetic, magnetic quantum tunneling and spin-glasslike behavior etc. [1].

The cubic spinel ferrites structure AB_2O_4 is a face-center cubic structure based on the oxygen ions. There are eight formula units of each spinel cubic unit cell. And it contains 64 tetrahedral sites (A sites) and 32 octahedral sites (B sites) in each spinel cubic unit cell. So, the chemical and physical properties of ferrite nanopowders are greatly influenced by the formula and structure, which are sensitive to the preparation methods [2]. Different kinds of cations can be situated in the structure of AB_2O_4 in tetrahedral and octahedral sites to change its properties. The chemical and physical properties of cubic spinel ferrites can be tuned systematically by changing the kinds of cations with the same spinel cubic structure [3–5].

There are some researchers have investigated the influence of Al concentration on the properties of the spinel ferrite, such as Ni ferrite [6, 7], MnNiZn ferrite [8], Li ferrite [9], Co ferrite [10–12] and NiZn ferrite [13, 14]. The effects of Al substitution on the properties of the NiZnCo bulk ferrite with lower sintered temperature are investigated in the previous work [15]. However, there are no reports on the effects of Al substitution on the structural, magnetic and dc electrical properties of the NiZnCo ferrite nanopowders.

According to the above reasons, Al substituted NiZnCo ferrite nanopowders were prepared by sol–gel auto-combustion method because it has mainly three advantages. To start with, it can use inexpensive precursors. In addition, it is a simple preparation method. Finally, it can obtained well dispersed homogenous, nano-sized and highly reactive ferrite powder with low sintering temperature [16, 17]. Compared with the bulk materials, there are some different efforts of Al substitution on the properties of NiZnCo ferrite nanopowders. Especially the temperature dependence of dc resistivity can be divided into two regions, including the metallic conduction part and semi-conduction part. So, the influence of Al substitution on the structural and electromagnetic properties of NiZnCo ferrite nanopowders are studied.

✉ Xiao-Xi Zhong
xiaoxi_zhong@163.com

[1] Sichuan Province Key Laboratory of Information Materials and Devices Application, College of Optoelectronic Technology, Chengdu University of Information Technology, Chengdu 610225, People's Republic of China

2 Experimental procedures

2.1 Preparation process

The ferrite nanopowders samples with chemical formula $Ni_{0.4}Zn_{0.5}Co_{0.1}Al_xFe_{2-x}O_4$ ($x = 0$, 0.05, 0.10, 0.15, 0.20) were prepared by sol–gel auto-combustion method. The stoichiometric quantities of analytical grade $Ni(CH_3COO)_2{\cdot}4H_2O$, $Zn(CH_3COO)_2{\cdot}2H_2O$, $Co(NO_3)_2{\cdot}6H_2O$, $Fe(NO_3)_3{\cdot}9H_2O$ and $Al(NO_3)_3{\cdot}9H_2O$ were used as raw materials. The nitrate were dissolved and stirred in deionization water. After the nitrates complete dissolution, the citric acid was added to the dissolved solution and the molar concentration ratio of $C_6H_8O_7{\cdot}H_2O$ and nitrates was taken as three to one. Then, the solution form the gel precursors after stirring for 3 h at 80 °C. The pH value is adjusted to 7 with the aqueous ammonia-solution at room temperature. The dry gel precursor was obtained after the solution drying at 90 °C in the furnace. Finally, the ferrite nanopowders is obtained when the dried gel was burned in self-propagation combustion.

2.2 Characterization and property measurements

The thermal decomposition of the as-prepared precursor was analyzed by Shimadzu DTG-60 thermal analyzer. The phase analysis of the nanopowders was measured by DX 2700 X-ray diffractometer at room temperature. The *M–H* loops of samples were performed at room temperature by TOEI VSM-5S-15 vibrating sample magnetometer. The *M–T* curves of samples were obtained by Lakeshore model 7304 vibrating sample magnetometer from room temperature to 500 °C. The temperature dependence of direct current resistivity was performed by Keithley 6517B high resistance meter from room temperature to 300 °C.

3 Results and discussion

3.1 Thermal decomposition of the as-prepared precursor

The minimum calcination temperature of the complete decomposition process can be determined by the thermal behavior measurements of the dried precursors [18]. The DTA-TG curves in air for the dried gel precursor of $Ni_{0.4}Zn_{0.5}Co_{0.1}Al_{0.1}Fe_{1.9}O_4$ are shown in Fig. 1. The endothermic peaks before 200 °C due to the evaporation of water molecules. The weight loss is about 14%. The exothermic peak at about 220 °C is attributed to the decomposition of precursor and ferrite formation with CO_2, N_2, and H_2O gas releasing, and the weight loss is about 65%. This sudden decomposition of the precursor is obtained in other systems [18, 19]. Furthermore, an exothermic peak obtained at about 355 °C in DTA curve is attributed to the oxidative decomposition of the surplus nitrate and organic substance. The weight loss is about 4.5%. It is noticed that there is no obvious weight loss obtained when the temperature is more than 430 °C.

3.2 Structural properties

Figure 2 shows the XRD patterns of $Ni_{0.4}Zn_{0.5}Co_{0.1}Al_xFe_{2-x}O_4$ ferrite nanopowders. It indicates that there is ZnO secondary impurity phase when $x \geq 0.10$. The lattice constant (a), nanopowder size (D) and X-ray theoretical density (d_x) are calculated

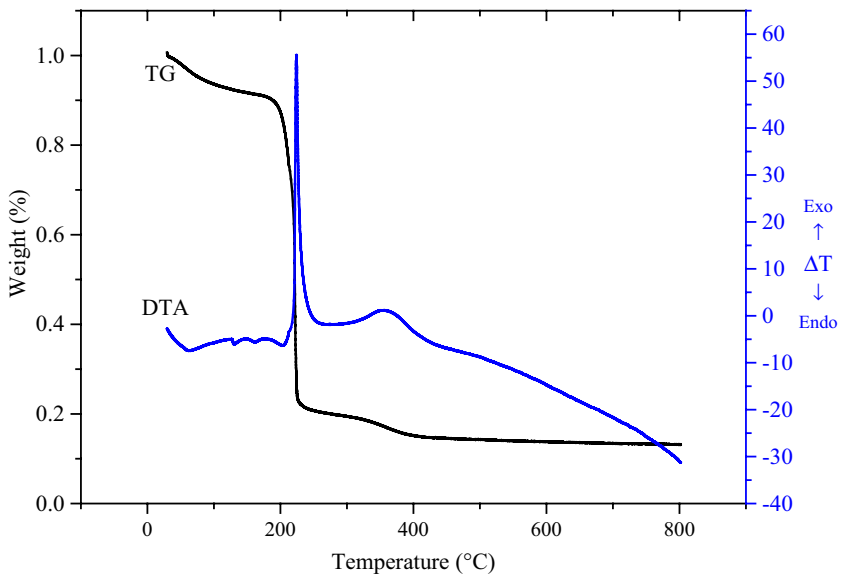

Fig. 1 DTA–TG curves of precursors with $Ni_{0.4}Zn_{0.5}Co_{0.1}Al_{0.1}Fe_{1.9}O_4$

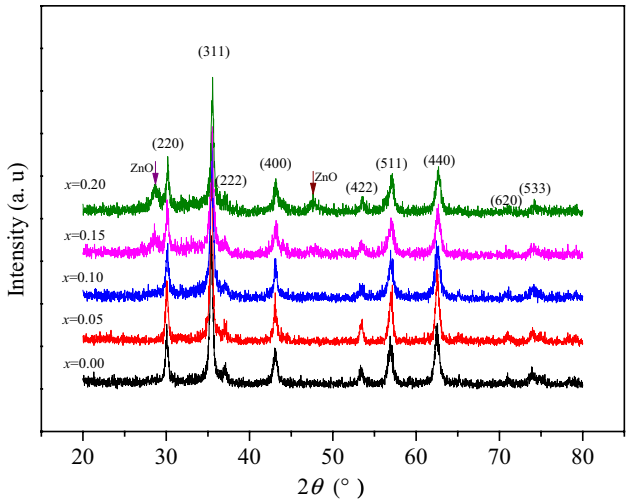

Fig. 2 XRD patterns of $Ni_{0.4}Zn_{0.5}Co_{0.1}Al_xFe_{2-x}O_4$ ferrite nanopowders

by XRD data and the results are listed in Table 1. *a, D* and d_x decrease from 0.8406 to 0.8372 nm, 26.0 to 20.1 nm and 5.32 to 5.25 g/cm^3, respectively.

The lattice parameter (a) of the samples is calculated using the relation [20]:

$$a_{exp} = d_{hkl}\sqrt{h^2 + k^2 + l^2} \quad (1)$$

where ($h\ k\ l$) are the Miller indices and d_{hkl} is the inter-planar spacing. The average crystallite size is calculated according to Debye–Scherrer equation [20–22]:

$$D = \frac{0.9\lambda}{\beta \cos\theta} \quad (2)$$

where λ is wavelength of the X-ray radiation, β is the full width at half maxima in radian and θ is the Bragg's angle. The X-ray densities (d_x) are calculated using the following relation [23, 24]:

$$d_x = \frac{8M_W}{N_A a^3} \quad (3)$$

where M_W is the molecular weight; N_A is the Avogadro's parameter and a is the lattice parameter.

Table 1 Variations of lattice constant (a), crystallite size (D) and X-ray theoretical density (d_x) of $Ni_{0.4}Zn_{0.5}Co_{0.1}Al_xFe_{2-x}O_4$ ferrite nanopowders

x	0.00	0.05	0.10	0.15	0.20
a (nm)	0.8406	0.8394	0.8392	0.8384	0.8372
D (nm)	26.0	24.1	22.2	21.3	20.1
d_x (g/cm^3)	5.32	5.31	5.28	5.26	5.25

The lattice constant decrease with Al substitution increasing because the bigger ionic radius of Fe^{3+} ions (0.067 nm) is replaced by smaller Al^{3+} ions (0.051 nm) which results in the constriction in the dimensions of unit cell. The decrease of D with Al substitution increasing demonstrates that Al substitution restrains the crystal growth. Similar result in grain size with Al substitution increasing is also observed in MnZn, Co, Ni, and NiZn ferrite system [7, 9, 12, 14, 25]. The reduction of molecular weight from 237.8 to 232.0 is due to the fact that Fe^{3+} ions with higher atomic weight (55.845) is substituted by lower atomic weight Al^{3+} ions (26.982). Consequently, it reduces the X-ray theoretical density.

3.3 Magnetic properties

The hysteresis loops (M–H) of $Ni_{0.4}Zn_{0.5}Co_{0.1}Al_xFe_{2-x}O_4$ ferrite nanopowders are shown in Fig. 3. Figure 4 shows the variation of saturation magnetization (Ms) and coercivity (Hc) of ferrite nanopowders as a function of Al substitution (x). It shows that Ms has the maximum value (75.43 emu/g) and Hc reaches the minimum value (81.59 Oe) when Al substitution (x) is 0.10.

For spinel ferrite, the composition, cation distribution, structure, grain size, defects and internal strain can influence the magnetic properties. Based on Néel's two sublattice model of ferrimagnetisms [26], the magnetic moment of spinel ferrite can be determined by $M = |M_B - M_A|$, where M_A is the magnetization of A-site and M_B is the magnetization of B-site. For bulk ferrite, the non-magnetic Al^{3+} ions (0 μ_B) replace the magnetic Fe^{3+} ions (5 μ_B) at B-sites will reduce M_B and hence make the magnetic moment decrease. This result has been obtained in the previous work concerned the bulk NiZnCo ferrite [15]. However, compared with the previous work [15], Ms

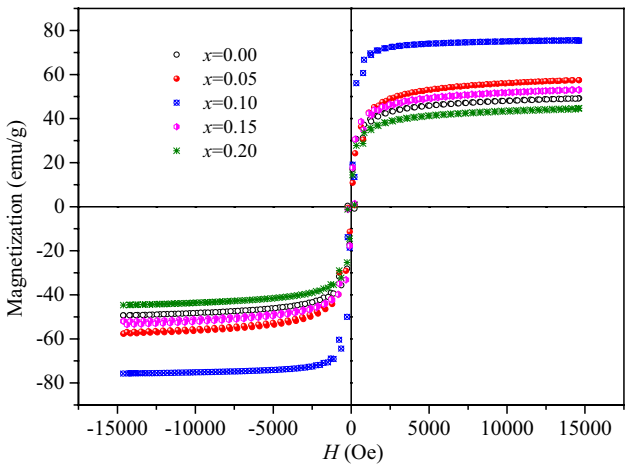

Fig. 3 M–H loops of $Ni_{0.4}Zn_{0.5}Co_{0.1}Al_xFe_{2-x}O_4$ ferrite nanopowders

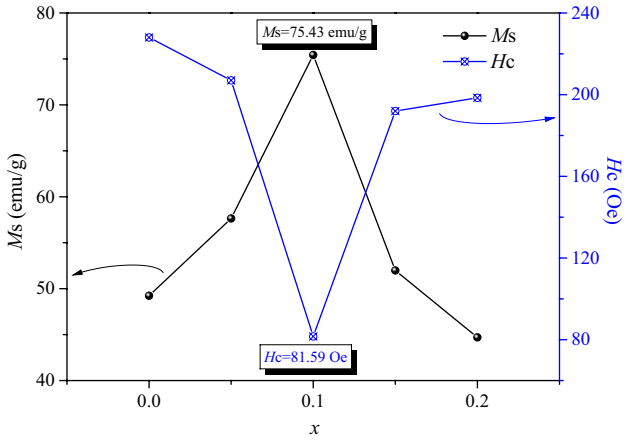

Fig. 4 Variation of *M*s and *H*c with *x* for $Ni_{0.4}Zn_{0.5}Co_{0.1}Al_xFe_{2-x}O_4$ ferrite nanopowders

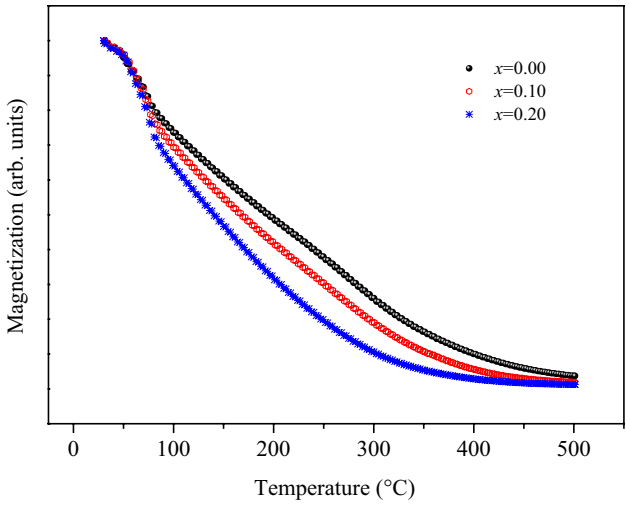

Fig. 5 The variation of magnetization of $Ni_{0.4}Zn_{0.5}Co_{0.1}Al_xFe_{2-x}O_4$ (x = 0, 0.10, 0.2) ferrite nanopowders as a function of temperature

of NiZnCo nanopowders increases with Al substitution increasing when $x \leq 0.10$ which is shown in Figs. 3 and 4. The different variation of *M*s with Al substitution is mainly because the cation distribution in nanostructured ferrites are different from that in the bulk ferrites [27]. According to the investigation of R. S. Biasia, H. F. Santosa [7], Al^{3+} ion can enter A-site in NiAl ferrite nanoparticles which can decrease M_A for lower concentration. In addition, the magnetocrystalline anisotropy constant (K_1) decrease due to the fact that the non-magnetic Al^{3+} ions (0 μ_B) replace magnetic Fe^{3+} ions (5 μ_B) can enhance the value of *M*s. However, excessive magnetic Fe^{3+} ions are replaced by nonmagnetic Al^{3+} ions in B-site will reduce M_B. It results in the decrease of *M*s. Furthermore, the decrease of crystallite size and the exist of ZnO impurity phase with excessive Al substitution also can make *M*s decrease. Eventually, *M*s decreases with the increase of Al substitution when $x > 0.10$.

Figure 4 shows the variation of *H*c with Al substitution (*x*). It indicates that *H*c decreases with Al substitution increasing when $x \leq 0.10$, and then raises when $x > 0.10$. For cubic spinel ferrite, *H*c is related to K_1 and *M*s by the relation: $Hc \propto K_1/Ms$. Based on this relation, *H*c decreases with K_1 decrease and *M*s increase when $x \leq 0.10$. However, *H*c increases with Al substitution increasing when $x > 0.10$ mainly because the excessive non-magnetic Al ions lead to the decrease of *M*s.

The variation of magnetization of $Ni_{0.4}Zn_{0.5}Co_{0.1}Al_xFe_{2-x}O_4$ ($x = 0, 0.10, 0.2$) ferrite nanopowders as a function of temperature is shown in Fig. 5. This indicates that the Néel temperature (T_N) decreases with Al substitution (*x*) increment, which mainly due to the fact that the replacement of magnetic Fe^{3+} ions by the nonmagnetic Al^{3+} ions reduces the superexchange interaction.

3.4 Electrical properties

The temperature dependence of dc resistivity ρ_d for the $Ni_{0.4}Zn_{0.5}Co_{0.1}Al_xFe_{2-x}O_4$ ($x = 0$-0.20) ferrite nanopowders is shown in Fig. 6a. All samples show the metal–semiconductor (M–S) transition behavior at a specific temperature with a resistivity peak which called transition temperature (T_p). Under the temperature of T_p, ρ_d shows the metallic conduction mechanism and increases with the temperature. But, when the temperature is above T_p, ρ_d shows the intrinsic semi-conduction mechanism and follows an exponential decay with temperature increasing. In fact, the ρ_d–T curves mainly contain the metallic conduction region which is dominated by the scattering effect with lattice vibration and semi-conduction region which is dominated by the electrons hopping between Fe^{2+} and

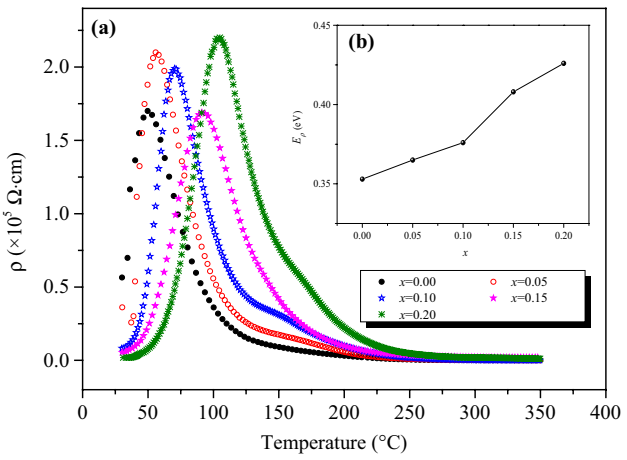

Fig. 6 Temperature dependence of ρ_d (**a**) and variation of E_ρ with *x* (**b**) for $Ni_{0.4}Zn_{0.5}Co_{0.1}Al_xFe_{2-x}O_4$ ferrite nanopowders

Fe^{3+} ions at B-sites [28]. This well agrees with the electrical conductivity properties for impurity semiconductor. For the spinel ferrites, electrons hopping between Fe^{2+} and Fe^{3+} ions plays a vital role of intrinsic excitation. The intrinsic excitation is expected to increase the charge carrier concentration to reduce ρ_d in the semi-conduction region. But the lattice vibration scattering effect enhances with temperature increasing will obstruct the electron conduction and reduce the dc drift mobility in the metallic conduction region. In practice, T_p is used to separate the metallic conduction and semi-conduction regions mainly depends upon the competition between lattice vibration scattering and intrinsic excitation. T_p increases with Al substitution in the present work.

In the semi-conduction region, the temperature dependence of dc resistivity follows the Arrhenius equation $\rho_d = \rho_0 \exp\left(E_\rho/kT\right)$, where ρ_d is the resistivity at temperature T, ρ_0 is a constant which equals to the resistivity at infinitely high temperature, k is Boltzman's constant, and E_ρ is activation energy [29]. The exponential decay of ρ_d with the temperature increasing demonstrates that the semiconductor behavior of ferrites. Conduction in spinel ferrites can be stated by Verwey's hopping mechanism [30]. According to it, the electronic conduction in spinel ferrites is formed by the electrons hopping between ions of the same element with different valance state, distributed randomly over the same lattice sites. Figure 6a shows that ρ_d increases with Al substitution increasing in semi-conduction region. This mainly due to the fact that the predominantly conduction mechanism of spinel ferrites is the electrons hopping between $Fe^{2+} \leftrightarrow Fe^{3+} + e^-$ [28]. With the increase of Al substitutes Fe, Fe^{2+} ions will decrease which restricts the electron hopping between Fe^{3+} and Fe^{2+} ions and then it leads to the increase of ρ_d.

The hopping probability is also influenced by the activation energy [31]. In the semi-conduction region, the activation energies E_ρ can be obtained by the Arrhenius equation [32]. Figure 6b indicates that the values of activation energies increased from 0.353 eV ($x=0$) to 0.426 eV ($x=0.20$), which indicates that E_ρ is influenced by Al substitution. E_ρ is associated with the electrical energy barrier during electrons hopping. And the Fe^{3+} ions are being replaced by the different element ions at the same lattice sites will results in much higher electrical energy barrier. So, E_ρ increases with Al substitution increasing. And then the electrons hopping needs much higher thermal energy with the increase of E_ρ which results in the increase of T_p.

4 Conclusions

$Ni_{0.4}Zn_{0.5}Co_{0.1}Al_xFe_{2-x}O_4$ ($0 \le x \le 0.20$) ferrite nanopowders were prepared by sol–gel auto-combustion method. The effects of Al substitution on the structural and electromagnetic properties have been studied. DTA–TG results indicate that the decomposition of the gel occurs suddenly at about 220 °C. The a, D and d_x of ferrite nanopowders decrease from 0.8406 to 0.8372 nm, 26.0 to 20.1 nm and 5.32 to 5.25 g/cm^3, respectively. Ms increases with the increase of Al substitution when $x \le 0.10$, and then decreases when $x > 0.10$. Hc decreases with the increase of Al substitution when $x \le 0.10$, and then increases when $x > 0.10$. Ms has the maximum value (75.43 emu/g) and Hc reaches the minimum value (81.59 Oe) when Al substitution (x) is 0.10. The Néel temperature (T_N) decreases with the increase of Al substitution. The temperature dependence of ρ_d for the ferrite nanopowders follows the impurity semiconductor, and T_p increases with Al substitution because of the increase of E_ρ with the increase of Al substitution. Furthermore, ρ_d increases in semi-conduction region with Al substitution increasing.

Acknowledgements This work was supported by the National Natural Science Foundation of China under Grant No. 51502025.

References

1. M.S. Khandekar, R.C. Kambale, J.Y. Patil, Y.D. Kolekar, S.S. Suryavanshi, Effect of calcination temperature on the structural and electrical properties of cobalt ferrite synthesized by combustion method. J. Alloys Compd. **509**, 1861–1865 (2011)
2. F. Li, J.J. Liu, D.G. Evans, X. Duan, Stoichiometric synthesis of pure MFe_2O_4 (M = Mg, Co, and Ni) spinel ferrites from tailored layered double hydroxide (hydrotalcite-like) precursors. Chem. Mater. **16**, 1597–1602 (2004)
3. S.T. Alone, S.E. Shirsath, R.H. Kadam, K.M. Jadhav, Chemical synthesis, structural and magnetic properties of nano-structured Co-Zn-Fe-Cr ferrite. J. Alloys Compd. **509**, 5055–5060 (2011)
4. L. Huan, X. Tang, H. Su, H. Zhang, Y. Jing, Effects of SiO_2 concentration on the DC-bias-superposition characteristics of the NiCuZn ferrites. J. Mater. Sci.: Mater. Electron. **26**, 3275–3281 (2015)
5. M. Ušáková, J. Lukáč, R. Dosoudil, V. Jančárik, A. Grusková, E. Ušák, J. Sláma, J. Šubrt, Influence of Cu^{2+} ions on structural and magnetic properties of NiZn ferrites. J. Mater. Sci.: Mater. Electron. **18**, 1183–1189 (2007)
6. M. Mozaffari, J. Amighian, Preparation of Al-substituted Ni ferrite powders via mechanochemical processing. J. Magn. Magn. Mater. **260**, 244–249 (2003)
7. R.S. Biasi, H.F. Santos, Cation distribution, saturation magnetization and magnetocrystalline anisotropy of mixed ferrite $NiAl_xFe_{2-x}O_4$ nanoparticles. Ceram. Int. **43**, 4557–4561 (2017)
8. A.A. Sattar, H.M. El-Sayed, K.M. El-Shokrofy, M.M. El-Tabey, Improvement of the magnetic properties of Mn-Ni-Zn Ferrite by the non magnetic Al-Ion substitution. J. Appl. Sci. **3**, 162–168 (2005)
9. M.A. Dar, K.M. Batoo, V. Verma, W.A. Siddiqui, R.K. Kotnala, Synthesis and characterization of nano-sized pure and Al-doped lithium ferrite having high value of dielectric constant. J. Alloys Compd. **493**, 553–560 (2010)
10. L. Kumar, M. Kar, Influence of Al^{3+} ion concentration on the crystal structure and magnetic anisotropy of nanocrystalline spinel cobalt ferrite. J. Magn. Magn. Mater. **323**, 2042–2048 (2011)

11. A.T. Raghavender, K.M. Jadhav, Dielectric properties of Al-substituted Co ferrite nanoparticles. Bull. Mater. Sci. **32**, 575–578 (2009)
12. B.K. Kuanr, S.R. Mishra, L. Wang, D. Conte, D. Neupane, V. Veerakumar, Z. Celinski, Frequency and field dependent dynamic properties of $CoFe_{2-x}Al_xO_4$ ferrite nanoparticles. Mater. Res. Bull. **76**, 22–27 (2016)
13. M. Hashim, S. Kumar, S. Ali, B.H. Koo, H. Chung, R. Kumar, Structural, magnetic and electrical properties of Al^{3+} substituted Ni–Zn ferrite nanoparticles. J. Alloys Compd. **511**, 107–114 (2012)
14. A.A. Birajdar, S.E. Shirsath, R.H. Kadam, M.L. Mane, D.R. Mane, A.R. Shitre, Permeability and magnetic properties of Al^{3+} substituted $Ni_{0.7}Zn_{0.3}Fe_2O_4$ nanoparticles. J. Appl. Phys. **112**, 053908 (2012)
15. L.Z. Li, X.X. Zhong, R. Wang, X.Q. Tu, L. He, R.D. Guo, Z.Y. Xu, Structural, magnetic and electrical properties in Al–substitued NiZnCo ferrite prepared via the sol–gel auto-combustion method for LTCC technology. RSC Adv. **7**, 39198 (2017)
16. M. Hashim, S. Alimuddin, S.E. Kumar, R.K. Shirsath, J. Kotnalad, R. Shah, Kumar, Influence of Cr^{3+} ion on the structural, ac conductivity and magnetic properties of nanocrystalline Ni–Mg ferrite. Ceram. Int. **39**, 1807–1819 (2013)
17. M. Han, C.R. Vestal, Z.J. Zhang, Quantum couplings and magnetic properties of $CoCr_xFe_{2-x}O_4$ ($0 < x < 1$) spinel ferrite nanoparticles synthesized with reverse Micelle method. J. Phys. Chem. B **108**, 583–587 (2004)
18. W.A. Bayoumy, M.A. Gabal, Synthesis characterization and magnetic properties of Cr-substituted NiCuZn nanocrystalline ferrite. J. Alloys Compd. **506**, 205–209 (2010)
19. M.A. Gabal, Y.M.A. Angari, Effect of chromium ion substitution on the electromagnetic properties of nickel ferrite. Mater. Chem. Phys. **118**, 153–160 (2009)
20. B.D. Cullity, *Elements of X-ray Diffraction* (Addison Wesley Publishing, Reading, 1959)
21. M.H. Mahmoud, C.M. Williams, J. Cai, I. Siu, J.C. Walker, Investigation of Mn-ferrite films produced by pulsed laser deposition. J. Magn. Magn. Mater. **261**, 314–318 (2003)
22. M.H. Ibrahim, M.S. Seehra, G. Srinivasan, Observations of magnetization reversal and magnetic clusters in copper ferrite films. J. Appl. Phys. **75**, 6822–6824 (1994)
23. S. Amiri, H. Shokrollahi, Magnetic and structural properties of RE doped Co-ferrite (RE = Nd, Eu, and Gd) nano-particles synthesized by co-precipitation. J. Magn. Magn. Mater. **345**, 18–23 (2013)
24. E.R. Kumar, R. Jayaprakash, S. Kumar, Effect of annealing temperature on structural and magnetic properties of manganese substituted $NiFe_2O_4$ nanoparticles. Mater. Sci. Semicond. Process. **17**, 173–177 (2014)
25. M.A. Gabal, A.M. Abdel-Daiem, Y.M. Angari, I.M. Ismail, Influence of Al-substitution on structural, electrical and magnetic properties of Mn–Zn ferrites nanopowders prepared via the sol–gel auto-combustion method. Polyhedron **57**, 105–111 (2013)
26. D.F. Wan, X.L. Ma, *The Physics of Magnetism* (UESTC Press, Chengdu, 1994)
27. N. Ponpandian, A. Narayanasamy, C.N. Chinnasamy, N. Sivakumar, J.M. Greneche, K. Chattopadhyay, K. Shinoda, B. Jeyadevan, K. Tohji, Néel temperature enhancement in nanostructured nickel zinc ferrite. Appl. Phys. Lett. **86**, 192510 (2005)
28. L. Peng, L.Z. Li, X.X. Zhong, Y. Hu, X.Q. Tu, R. Wang, Magnetic, electrical, and dielectric properties of La-Cu substituted Sr-hexaferrites for use in microwave LTCC devices. J. Alloys Compd. **665**, 31–36 (2016)
29. U.V. Chhaya, R.G. Kulkarni, Metal-insulator type transition in aluminum and chromium co-substituted nickel ferrites. Mater. Lett. **39**, 91–96 (1999)
30. E.J.W. Verwey, J.H. De Boer, Cation arrangement in a few oxides with crystal structures of the spinel type. Rec. Trav. Chim. Pays-Bas **55**, 531–540 (1936)
31. A. Lakshman, P.S.V.S. Rao, B.P. Rao, K.H. Rao, Electrical properties of In and Cr substituted magnesium-manganese ferrites. J. Phys. D **38**, 673–678 (2005)
32. A. Thakur, P. Mathur, M. Singh, Study of dielectric behavior of Mn-Zn nano ferrites. J. Phys. Chem. Solids **68**, 378–381 (2007)